

# Fingering instabilities of exothermic reaction-diffusion fronts in porous media

S. Kalliadasis and J. Yang

*Department of Chemical Engineering, University of Leeds, Leeds LS2 9JT, United Kingdom*

A. De Wit

*Service de Chimie Physique and Centre for Nonlinear Phenomena and Complex Systems, CP 231, Université Libre de Bruxelles, 1050 Brussels, Belgium*

(Received 23 December 2003; accepted 6 February 2004; published online 5 April 2004)

We consider the density fingering of exothermic autocatalytic fronts in vertically oriented Hele-Shaw cells with chemical reactions whose solutal and thermal contributions to density changes have opposite signs. Using the Darcy–Boussinesq equations we examine the influence of the competition between solutal and thermal density changes on the linear stability of traveling fronts and the fully nonlinear dynamics. Ascending fronts are characterized by standard Rayleigh–Taylor fingering dispersion curves and in the nonlinear stage of the instability they feature thermal plumes. Descending fronts on the other hand behave strikingly differently as they can feature for some values of the parameters Turing-type dispersion curves and stationary patterns with fingers of constant amplitude and wavelength. © 2004 American Institute of Physics.

[DOI: 10.1063/1.1689912]

## I. INTRODUCTION

Chemical reactions can change the density of a solution either by modifying the total volume of products versus reactants or by releasing or consuming heat. These two effects provide a solutal and/or thermal contribution to the total density change. Across a moving autocatalytic reaction–diffusion front traveling along the direction of gravity, such a jump in density can lead to a Rayleigh–Taylor instability if the heavier solution is placed on top of the lighter one in the gravity field. This hydrodynamic instability then interacts with the chemical reaction affecting the propagation speed of the front and leading eventually to a complex spatiotemporal dynamics which is dramatically different from the one observed for pure density fingering in the absence of reactions.

For the nitric acid-iron(II) system, Bazsa and Epstein noted that, reaction fronts travel several times more rapidly going down a narrow tube than going up<sup>1</sup> (if the front is not laterally extended, the hydrodynamic instability does not develop). They suggested that this behavior is due to the effects of convection induced by the exothermicity of the reaction. Nagypál *et al.*<sup>2</sup> have analyzed in detail the same system, as well as the chlorite–thiosulfate reaction, showing experimentally that the velocity of the up or down going fronts depends on both thermal and solutal contributions to density. Pojman and Epstein<sup>3</sup> were the first who started to classify autocatalytic chemical reactions depending on the respective sign of the thermal and solutal contributions to density changes. If both effects are cooperative and lead to a decrease of the density behind the front, only up going fronts should be unstable due to stratification of cold heavy reactants on top of hotter and lighter products. According to the Pojman–Epstein model, simple convection is then expected. This case has been analyzed experimentally in the iodate-arsenous acid

(IAA) system, for which typically ascending fronts indeed feature buoyancy driven convection.<sup>4–7</sup>

When heat and solutal effects are in competition, we expect intuitively a possible instability for both up and down going fronts.<sup>3</sup> In this case, upward moving fronts correspond to a lighter solution on top of a heavy one, but as the products are hotter because of the reaction exothermicity, one expects that, if sufficient heat is produced, the planar fronts might become unstable. Downward moving fronts on the other hand consist of a heavy fluid on top of lighter solution, a buoyantly unstable solutal stratification giving rise to convection and fingering.<sup>8,9</sup> Nevertheless, for a large heat production, the products are also hotter and one might imagine that complete stabilization of downward moving fronts could result. Competition between such thermal and solutal buoyancy driven convection has been studied experimentally in the iron(II)–nitric acid,<sup>1,2,10</sup> the chlorite–thiosulfate,<sup>2</sup> the chlorate–sulfite,<sup>11</sup> the chlorite–thiourea,<sup>12</sup> the bromate–sulfite<sup>13</sup> and Belousov–Zhabotinsky<sup>14</sup> reactions and the traveling fronts of addition polymerization.<sup>15,16</sup> The explanations used by these authors to understand the observed dynamics are based on intuitive arguments which also invoke double-diffusive convection<sup>3,17,18</sup> related to differential diffusivity of heat and mass.

From the theoretical point of view, a number of studies have examined the influence of heat effects on the hydrodynamic stability of reaction fronts. Edwards *et al.*<sup>19</sup> addressed the role of density variations induced by the exothermicity of the reaction on the onset of convection for autocatalytic fronts. These authors coupled the Navier–Stokes equation with a buoyancy term to a convection–diffusion equation for the temperature. No kinetic term was involved and a flat front approximation was made. They studied the stability of laterally unbounded ascending fronts with respect to the ther-

mally induced density jump and they obtained the critical wavelength for the onset of convection and the growth rates near criticality. Further work under the same assumptions was carried out to investigate the limits of infinite and zero thermal diffusivity in bounded systems,<sup>20</sup> the case of finite diffusivity<sup>21,22</sup> as well as the possible transitions to axisymmetric versus symmetric modes at onset.<sup>23</sup> However, in these studies, heat effects influence only ascending fronts heated from below and there is no interplay between chemistry and heat production as no chemical kinetics is involved.

The onset of convection for an exothermic propagating front where now the energy equation is coupled to an equation for the depth of conversion for a one-step chemical reaction was examined in Refs. 24 and 25. In these studies, the kinetic constant of the reaction depends exponentially on temperature but the density jump at the interface is related solely to the temperature difference across the front. It was shown that convection can occur, not only for ascending fronts but for descending fronts also, the latter instability being possible only due to the interaction between the chemical reaction with the hydrodynamics. However, no solutal contributions to the density were taken into account. The nonlinear competition between both effects has been analyzed by Belk *et al.*<sup>16</sup> for photopolymerization fronts propagating perpendicularly to the gravity direction. The only work we are aware of in which both thermal and solutal contributions to density differences are taken into account to analyze buoyant convection of chemical fronts traveling along the direction of gravity, is that of Zhang *et al.*<sup>26</sup> who analyzed the complete system of reaction–diffusion–convection equations that govern the dynamics of the exothermic Belousov–Zhabotinsky reaction. They showed that both up and down going fronts are affected by the heat generated by the reaction, although they observed that the heat of reaction alone was too weak to destabilize the fronts.

Recently, Yang *et al.*<sup>9</sup> considered the buoyancy driven Rayleigh–Taylor instability of the chlorite–tetrathionate (CT) system in a vertical Hele–Shaw cell. They examined the linear stability of the isothermal traveling front of the CT system with respect to disturbances in the spanwise direction and demonstrated the existence of a preferred wavelength for the developed fingering instability. The linear stability analysis was found to be in excellent agreement with two-dimensional numerical simulations of the fully nonlinear system. These simulations showed also that at large times, some of the fingers merged leading to an overall coarsening of the fingering pattern, while in narrower systems the front evolves to one single finger traveling at a speed higher than the speed of the corresponding reaction–diffusion front in the absence of convection. We note that Yang *et al.* neglected thermal effects and focused on the study of the solutal density fingering. This allowed a comparison between the chemical front instability of the CT system and that of the IAA reaction<sup>27,28</sup> and it was found that both CT and IAA systems behave in a similar fashion with respect to the solutal buoyancy driven instability.

However, recent experiments with the CT system<sup>29</sup> show instabilities for the up going fronts. Such instabilities can only arise due to heat effects. Indeed, the CT system is

exothermic,<sup>30</sup> but for given reactant concentrations, the temperature rise may be neglected provided that the gap between the two plates of the Hele–Shaw cell is narrow. For higher concentrations and/or insulated walls or higher gapwidths, however, the heat losses to the surroundings are insufficient to maintain a constant temperature and therefore the temperature locally rises in the solution. As a consequence, the product solution becomes hotter than the reactants leading to the possibility of a thermal buoyancy driven instability for the up going front. On the contrary, for the downward moving front, the higher temperature on top will decrease the density of the product solution and hence might stabilize the traveling front (which is unstable because of solutal buoyancy effects).

The objective of the present study is to examine the density fingering of exothermic reaction–diffusion fronts considering antagonistic solutal and thermal contributions to density changes ( $\Delta\rho_S > 0$  while  $\Delta\rho_T < 0$ ) and to analyze the instabilities that can arise in the presence of a given kinetics. We focus on the chlorite–tetrathionate reaction as a typical example, for which experiments showing the importance of heat effects, have recently become available.<sup>29,30</sup> Although we use as a model the CT reaction, our analysis is quite generic and the formulation can be readily applied to any exothermic reaction–diffusion front with antagonist solutal and thermal density jumps.

Our model equations are based on the Darcy–Boussinesq approximation. We show that for fixed values of the kinetic parameters and Damköhler number, the system is governed by two parameters only, the dimensionless thermal expansion coefficient and the Lewis number. In the absence of convection, our base state is a planar traveling front for both concentration and temperature. We perform a linear stability of this front with respect to infinitesimal thermal–solutal buoyancy induced disturbances in the spanwise direction. We obtain the dispersion relation for the growth rate of these disturbances as a function of wavenumber for different values of the governing dimensionless groups. We analyze the stability properties of the system and we show that the instability mechanism involves a complex interplay between solutal–thermal effects, chemical reaction and double-diffusive phenomena. These last phenomena are only present for values of the Lewis number larger than unity.

For up going fronts, the dispersion curves are similar to those obtained in Rayleigh–Taylor fingering of reaction–diffusion fronts with a band of unstable wavenumbers that extends to zero so that small wavenumbers are always unstable and long wavenumbers always stable. Down going fronts on the other hand can feature, for certain values of the governing parameters, Turing-type dispersion curves characterized by a narrow band of unstable wavenumbers bounded by two neutral modes away from zero wavenumber. Hence, the coupling of solutal and thermal effects changes drastically the stability properties of reaction–diffusion fronts with regard to buoyancy induced fingering.

The nonlinear dynamics of both up and down going fronts is also studied by integrating numerically the fully nonlinear Darcy–Boussinesq system of equations. At the onset of the instability, the nonlinear simulations are in excel-

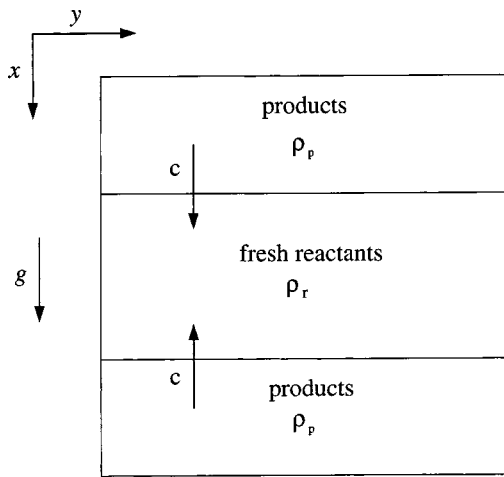


FIG. 1. Geometry of the reaction system in a Hele-Shaw cell. The reaction here is triggered either at the top or the bottom of the cell and the resulting chemical front travels downwards or upwards with velocity  $c$  invading the fresh reactants.

lent agreement with the predictions of our linear stability analysis. In the nonlinear regime the up going fronts feature thermal plumes of mushroom shape. At the same time we observe coarsening of the developed fingers in the course of time due to merging and shielding phenomena. As a result all fingers eventually merge into a single finger. The down going fronts on the other hand, can behave strikingly differently from the up going fronts. Depending on the values of the governing dimensionless groups, down going fronts can feature a new type of patterning in which the front develops a stationary cellular structure with fingers of constant amplitude and wavelength. Such stationary patterns have not been observed before in the context of fingering instabilities in porous media flows.

The paper is organized as follows. In Sec. II we formulate the model and introduce the various dimensionless parameters of the problem. In Sec. III, we construct the base state of our system in the form of a planar traveling front for both concentration and temperature. In Sec. IV, we perform a linear stability analysis of these planar fronts, we provide dispersion curves and we analyze the instability characteristics of both up and down going fronts. The nonlinear dynamics of both up and down going fronts is then examined in Sec. V. Finally, a discussion and conclusions are given in Sec. VI.

## II. PROBLEM DEFINITION, SCALINGS AND GOVERNING EQUATIONS

Figure 1 shows the problem definition. Our model system consists of a two-dimensional porous medium or Hele-Shaw cell with the gravity field along the streamwise direction. This is effectively the setup that has been studied experimentally by Bánsági *et al.*<sup>29</sup> for the CT reaction. The system is filled with the reacting species and the reaction is triggered either at the top or at the bottom of the system. The resulting chemical front moves downwards or upwards in-

vading the fresh reactants and leaving the products of the reaction behind it according to the stoichiometric equation for the particular reaction scheme.

We assume that in the absence of thermal effects, the density of the product solution is higher than that of the reactant solution. Hence, downward traveling fronts are buoyantly unstable and develop solutal density fingers in time while the upward traveling fronts are stable with respect to solutal effects.<sup>8,9</sup> However, the reaction is exothermic which produces a thermal contribution to density opposite to that of solutal effects.

The system is governed by the Darcy–Boussinesq equations

$$\nabla p = -\frac{\mu}{K}\underline{u} + \rho(\alpha, T)\underline{g}, \tag{1}$$

$$\nabla \cdot \underline{u} = 0, \tag{2}$$

$$\partial_t \alpha + \underline{u} \cdot \nabla \alpha = D_\alpha \nabla^2 \alpha - f(\alpha), \tag{3}$$

$$\rho_0 c_p [\partial_t T + \underline{u} \cdot \nabla T] = \kappa_T \nabla^2 T - \Delta H f(\alpha), \tag{4}$$

where  $\alpha$  is the concentration of the reactants and  $T$  the temperature.  $\mu$  and  $\rho$  are the viscosity and density of the fluid, respectively, and  $K$  the permeability of the porous medium. For thin Hele-Shaw cells,  $K = a^2/12$  with  $a$  the gapwidth between the two plates.  $D_\alpha$  is the diffusion coefficient of the reactants,  $\kappa_T$  is the thermal conductivity,  $c_p$  the constant pressure heat capacity,  $\rho_0$  the density of the pure solvent (e.g., water),  $\Delta H (<0)$  the heat of reaction and  $f(\alpha)$  the reaction rate. As the temperature changes involved in experiments are typically small ( $<10$  K), we assume here that all physical parameters are constant and do not depend on temperature. The density of the solution is

$$\rho(\alpha, T) = \rho_p - (\rho_p - \rho_r) \frac{\alpha}{\alpha_0} + \Gamma_T (T - T_0), \tag{5}$$

where  $\rho_p$  and  $\rho_r$  are the density of the products and reactants, respectively, at room temperature  $T_0$ ,  $\Gamma_T = \partial_T \rho(\alpha = 0, T_0)$  and  $\alpha_0$  is the initial concentration of the reactants. In the absence of thermal effects ( $T = T_0$ ), the density  $\rho_r$  of the reactant solution ( $\alpha/\alpha_0 = 1$ ) is smaller than the density  $\rho_p$  of the product solution ( $\alpha/\alpha_0 = 0$ ). Hence, the isothermal solutal density jump,  $\Delta \rho_S = (\rho_p - \rho_r)_S / \rho_p$  is positive, i.e., the products are heavier than the reactants while  $\Gamma_T < 0$ —heat effects make the fluid lighter.

To balance viscous and buoyancy forces we introduce the characteristic velocity

$$U = \frac{\Delta \rho_S g K}{\nu}, \tag{6}$$

where  $\nu = \mu/\rho_0$  is the kinematic viscosity of water. Balancing now convection with diffusion yields the characteristic length and time scales

$$L_h = \frac{D_\alpha}{U}; \quad \tau_h = \frac{D_\alpha}{U^2}. \tag{7}$$

We then non-dimensionalize Eqs. (1)–(5) by scaling velocity, length and time by  $U$ ,  $L_h$ , and  $\tau_h$ , respectively. Pres-

sure, density, concentration, and reaction rate are scaled with  $\mu D_\alpha/K$ ,  $(\rho_p - \rho_r)_S$ ,  $\alpha_0$  and  $\alpha_0/\tau_c$ , respectively, with  $\tau_c$  the characteristic chemical time scale which can be defined once the kinetics is specified. Temperature is scaled with  $(T - T_0)/T_0$ . The dimensionless governing equations then become

$$\nabla' p' = -\underline{u}' + (\rho'_p - \alpha' + \Gamma'_T T') \underline{i}_x, \quad (8)$$

$$\nabla' \cdot \underline{u}' = 0, \quad (9)$$

$$\partial_{t'} \alpha' + \underline{u}' \cdot \nabla' \alpha' = \nabla'^2 \alpha' - Da f'(\alpha'), \quad (10)$$

$$\partial_{t'} T' + \underline{u}' \cdot \nabla' T' = Le \nabla'^2 T' + \phi Da f'(\alpha'), \quad (11)$$

where the primes denote dimensionless variables.  $\underline{i}_x$  is the unit vector in the  $x$ -direction. The dimensionless thermal expansion coefficient is defined from  $\Gamma'_T = \Gamma_T T_0 / (\rho_p - \rho_r)_S$ . The Damköhler number,  $Da$ , is defined as the ratio of the hydrodynamic to the chemical time scale, i.e.,

$$Da = \frac{\tau_h}{\tau_c}, \quad (12)$$

while the Lewis number,  $Le$ , is defined as the ratio of the thermal to the molecular diffusivity

$$Le = \frac{D_T}{D_\alpha}, \quad (13)$$

where  $D_T = \kappa_T / \rho_0 c_p$  is the thermal diffusivity. Finally, the dimensionless reaction exothermicity,  $\phi$ , is defined as

$$\phi = \frac{|\Delta H| \alpha_0}{\rho_0 c_p T_0} \equiv \frac{\Delta T_b}{T_0}, \quad (14)$$

where  $\Delta T_b = T_b - T_0$  is the adiabatic temperature rise across the front (maximum temperature rise in the system) with  $T_b$  the adiabatic temperature.

To fix ideas let us consider the CT reaction.<sup>9</sup> This acid catalyzed reaction is taking place in slight excess of chlorite,  $\text{ClO}_2^-$ . The two main species of the CT reaction are the tetrathionate ions  $\alpha = [\text{S}_4\text{O}_6^{2-}]$  (the reactants), and the protons  $\beta = [\text{H}^+]$  (the products). As was pointed out by Yang *et al.*,<sup>9</sup> if we assume that the two species have the same diffusivity, the protons concentration  $\beta$  is stoichiometrically related to that of  $\alpha$ . The CT reaction scheme then reduces to a simple one-variable model (like the IAA system<sup>27</sup>) with a dimensional rate law

$$f(\alpha) = 36q \{ 2[\text{ClO}_2^-]_0 + 7(\alpha - \alpha_0) \} \alpha (\alpha_0 - \alpha)^2,$$

where  $q$  is the reaction rate constant of the overall reaction. The chemical time scale can then be defined as  $\tau_c = 1/(q\alpha_0^3)$  which yields the dimensionless rate

$$f'(\alpha') = 36\alpha'(1 - \alpha')^2(\kappa + 7\alpha'), \quad (15)$$

with  $\kappa = 2[\text{ClO}_2^-]_0/\alpha_0 - 7$ . We should emphasize here that the elimination of  $\beta$  from the rate law and the subsequent reduction of the CT system to a single-variable model, offers a simple prototype for the study of the coupling between reaction-diffusion processes and heat effects. The ideas developed here can be readily generalized and applied to other one-variable exothermic reaction-diffusion fronts.

We next define a new hydrostatic pressure gradient from  $\nabla'' p' = \nabla' p' - \rho'_p \underline{i}_x$ . In addition, we note that the transformation  $T \rightarrow \phi T$  scales away  $\phi$  from the energy equation and introduces a *modified* thermal expansion coefficient  $\gamma'_T = \phi \Gamma'_T$ . After dropping the primes, Eqs. (8)–(11) become

$$\nabla p = -\underline{u} + (\gamma_T T - \alpha) \underline{i}_x, \quad (16)$$

$$\nabla \cdot \underline{u} = 0, \quad (17)$$

$$\partial_t \alpha + \underline{u} \cdot \nabla \alpha = \nabla^2 \alpha - Da f(\alpha), \quad (18)$$

$$\partial_t T + \underline{u} \cdot \nabla T = Le \nabla^2 T + Da f(\alpha), \quad (19)$$

with  $f(\alpha) = 36\alpha(1 - \alpha)^2(\kappa + 7\alpha)$ , which are the basic equations for the analysis to follow. Notice that for  $\gamma_T = 0$  the hydrodynamic and thermal problems are decoupled. We recover in this limit the isothermal density fingering of the CT system as studied in Ref. 9.

We close this section with typical values of the dimensionless groups. To estimate the Lewis number we use the following values of parameters relevant for water at 20 °C:  $D_T = 1.429 \times 10^{-3} \text{ cm}^2/\text{s}$  and  $D_\alpha \sim 1.2 \times 10^{-4} \text{ cm}^2/\text{s}$ <sup>29</sup> which gives  $Le \sim 10$ . Notice that if we had a two-variable model for the chemical species  $\alpha$  and  $\beta$  (with the temperature field as the third variable) we would need  $D_\alpha = 2 \times 10^{-5} \text{ cm}^2/\text{s}$  for the tetrathionate ions and  $D_\beta = 1.2 \times 10^{-4} \text{ cm}^2/\text{s}$  for the protons. This would give a value  $Le \sim 70$  for water. In this study, however, we approximated the two-variable chemical system with one species (and temperature) and hence a value  $D_\alpha = 1.2 \times 10^{-4} \text{ cm}^2/\text{s}$  is more reasonable since it is the diffusion of the autocatalyst  $\beta$  that drives the chemical front. For the reaction exothermicity, we have  $\Delta T_b \sim 2$  to 3 K for the CT system<sup>29</sup> which with  $T_0 \sim 300$  K yields  $\phi \sim 0.01$ . It is precisely because of such a small value of  $\Delta T_b$  that we have assumed the kinetics of the CT reaction to be temperature-independent.

Finally, the thermal expansion coefficient can be estimated from its definition  $\Gamma'_T = \Gamma_T T_0 / (\rho_p - \rho_r)_S$ . This with  $\Gamma_T = (\partial_T \rho)_T \sim \Delta \rho_T \rho_0 / \Delta T$  where  $\Delta \rho_T = (\rho_p - \rho_r)_T / \rho_0$  gives  $\Gamma'_T \sim \Delta \rho_T T_0 / (\Delta \rho_S \Delta T)$ . We then need the density changes due to the thermal and solutal effects. Typical values are  $\Delta \rho_T \sim -5.9 \times 10^{-4}$  and  $\Delta \rho_S \sim 4.5 \times 10^{-4}$ .<sup>29</sup> Hence,  $\Gamma'_T \sim -100$  to  $-200$  so that the thermal expansion coefficient is quite large (note here that this coefficient should be negative since the density of water decreases with temperature above 4°C—we work here around 300 K). However, for the modified expansion coefficient we have  $\gamma'_T = \phi \Gamma'_T \sim O(1)$  because  $\phi$  is small. Note that from  $\Gamma'_T \sim \Delta \rho_T T_0 / (\Delta \rho_S \Delta T)$  with  $\Delta T \sim \Delta T_b$  we have  $\Gamma'_T \sim (1/\phi) \Delta \rho_T / \Delta \rho_S$  so that  $\gamma'_T \sim \Delta \rho_T / \Delta \rho_S$  and hence the dimensionless thermal expansion coefficient measures the thermal density change relative to the isothermal one. It is also important to emphasize here that scaling away  $\phi$  from the energy equation (effectively setting  $\phi = 1$  in this equation) implies that for fixed  $Da$  and  $\kappa$  the behavior of the system depends on two parameters only:  $Le$  and  $\gamma_T$ . We thus fix  $Da$  and  $\kappa$  to typical values for the CT system,  $Da = 0.001$  and  $\kappa = 1$ ,<sup>9</sup> and concentrate on the effect of varying  $Le$  and  $\gamma_T$ .



### III. TRAVELING FRONT

We now seek one-dimensional traveling front solutions  $(\alpha_s, T_s)$  propagating at constant speed  $c$  in the absence of convection. Setting  $\underline{u} = \underline{0}$  in (18) and (19) and introducing the Lagrangian coordinate  $z = x - ct$ , yields

$$-cd_z\alpha_s = d_z^2\alpha_s - Daf(\alpha_s), \tag{20}$$

$$-cd_zT_s = Led_z^2T_s + Daf(\alpha_s). \tag{21}$$

Adding now these two equations gives

$$d_z^2\alpha_s + cd_z\alpha_s + Led_z^2T_s + cd_zT_s = 0, \tag{22}$$

which can be integrated once and the integration constant can be determined from the boundary condition  $(\alpha_s, T_s) \rightarrow (1, 0)$  as  $z \rightarrow +\infty$ . We then have

$$d_z\alpha_s + Led_zT_s + c(\alpha_s + T_s - 1) = 0. \tag{23}$$

Application of the condition  $\alpha_s \rightarrow 0$  as  $z \rightarrow -\infty$  in the equation above then gives  $T_s \rightarrow 1$  as  $z \rightarrow -\infty$ . Notice that in the particular case  $Le = 1$ , (22) can be easily integrated to give  $\alpha_s + T_s = 1 + c'e^{-cz}$  where  $c'$  is an integration constant. But  $e^{-cz}$  blows up as  $z \rightarrow -\infty$ . This then implies that  $c' = 0$  which results in the simple relation  $T_s = 1 - \alpha_s$ .

Equations (21) and (22) can be converted into a three-dimensional dynamical system of the form

$$d_z\alpha_s = c(1 - \alpha_s - T_s) - Lev, \tag{23a}$$

$$d_zT_s = v, \tag{23b}$$

$$d_zv = \frac{1}{Le}[-cv - 36Da\alpha_s(1 - \alpha_s)^2(\kappa + 7\alpha_s)]. \tag{23c}$$

In the  $(\alpha_s, T_s, v)$  phase-plane, the front is a heteroclinic trajectory connecting the two fixed points  $(0, 1, 0)$  and  $(1, 0, 0)$  associated with the boundary conditions

$$z \rightarrow -\infty: \quad \alpha_s \rightarrow 0, \quad T_s \rightarrow 1,$$

$$z \rightarrow +\infty: \quad \alpha_s \rightarrow 1, \quad T_s \rightarrow 0.$$

We then utilize the numerical scheme developed in Ref. 9 to obtain the permanent-form traveling front solutions. The analysis here parallels the one given by Yang *et al.*<sup>9</sup> and the reader is referred to this study for details.

As with the isothermal CT system studied in our previous work, there exists a minimum speed  $c_{\min}$  such that a unique permanent-form traveling front exists for each  $c \geq c_{\min}$ . Of course this raises the question of front selection. Solving numerically the reaction-diffusion equations in time and space as an initial-value-problem indicates that the minimum speed front is always approached for large times, provided the initial condition is sufficiently localized in space. Hence the minimum speed front is the stable solution. Let us note that  $\alpha_s$  is independent of  $T_s$ —see (20)—and hence the minimum speed does not depend on  $Le$  and for given  $\kappa$  and  $Da$  it is fixed. Our computations indicate that for the values  $Da = 0.001$  and  $\kappa = 1$  used here,  $c_{\min} = 0.311$  in agreement with the relation  $c_{\min} = 9.833\sqrt{Da}$  given in Ref. 9 for  $\kappa = 1$ .

The temperature front on the other hand does depend on  $Le$  and becomes more spread out as  $Le$  increases. This is due to the fact that the Lewis number is effectively the ratio of

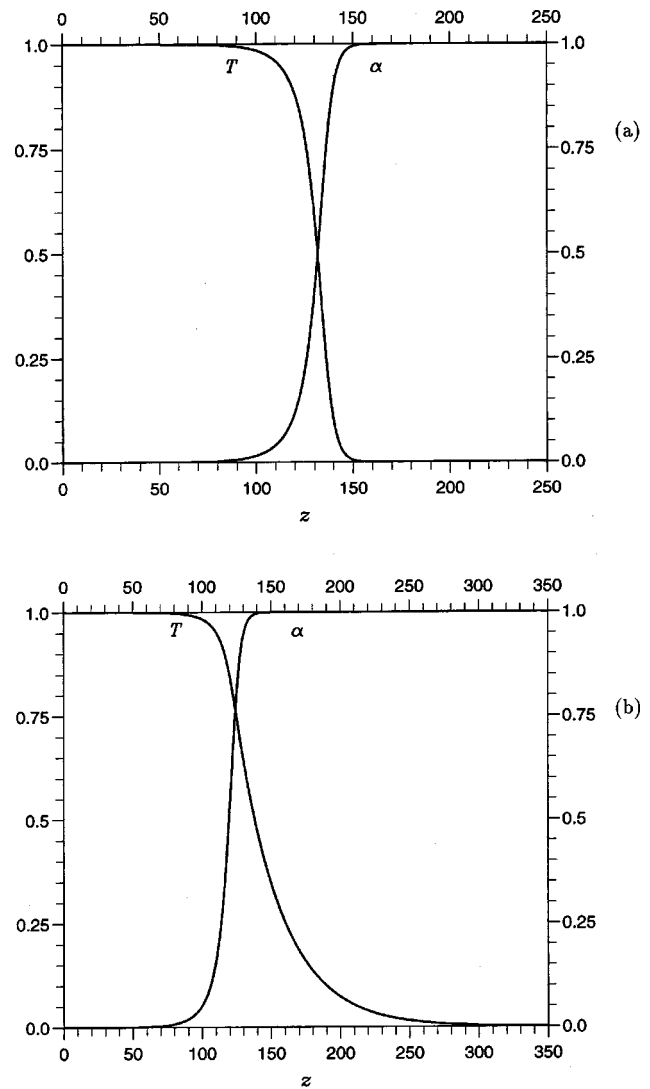


FIG. 2. Stationary traveling fronts for  $Da = 0.001$ ,  $\kappa = 1$  and two different values of the Lewis number.  $z = 0$  corresponds to either the top or the bottom of the cell. In both cases the front propagates from the left to the right; (a)  $Le = 1$ ; (b)  $Le = 10$ .

the thermal diffusion time scale to the molecular diffusion time scale. Hence, large  $Le$  implies that heat diffuses faster than concentration so that the width of the temperature front is much larger compared to that for the concentration front. Figures 2(a) and 2(b) depict the concentration–temperature front for two different values of the Lewis number. Figure 3 shows the variation of the width of the temperature front (defined as the domain in which  $T$  is in the interval  $[0.01, 0.99]$ ) as a function of  $Le$ . Finally, Fig. 4 depicts the density profile as a function of  $z$ , for two different values of the Lewis number. These profiles show that for isothermal systems, ( $\gamma_T = 0$ ), the density of the products is larger than that of the reactants. When  $|\gamma_T|$  increases, the heat released to the system increases and the products become hotter than the reactants. Their density then decreases while the density of the fresh reactants remains the same. Interestingly, for  $Le = 10$  and certain values of  $\gamma_T$ , the density profile across the front is nonmonotonic for both up and down going fronts.

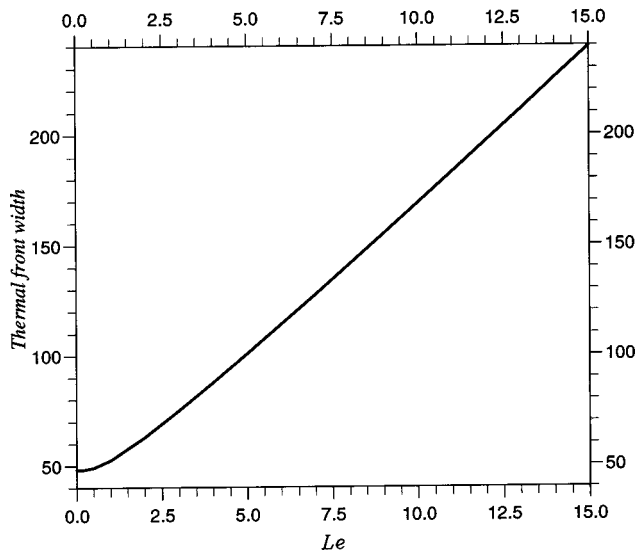


FIG. 3. Width of the temperature front as a function of Lewis number. The width is defined as the domain in which  $T$  takes on values in the interval  $[0.01, 0.99]$ .

IV. LINEAR STABILITY

A. Eigenvalue problem

We now examine the stability of the exothermic traveling front with respect to infinitesimal disturbances in the spanwise direction. In the moving frame, the steady state of Eqs. (16)–(19) is  $\underline{u} = \underline{u}_s + \underline{u}_1$ ,  $\alpha = \alpha_s + \alpha_1$ ,  $T = T_s + T_1$  and  $p = p_s + p_1$  with  $\underline{u}_1, \alpha_1, T_1, p_1 \ll 1$ . Linearizing (16)–(19) in the moving frame and utilizing (20) and (21) yields the evolution equations for the disturbances

$$d_z p_s = \gamma_T T_s - \alpha_s, \tag{24}$$

since  $\partial_y p_s = -w_s \equiv 0$ , with  $w$  the velocity in the  $y$ -direction, and hence the base state pressure distribution is only a function of  $z$ . The pressure profile can then be easily found by integrating (24) above. Let  $\underline{u} = \underline{u}_s + \underline{u}_1$ ,  $\alpha = \alpha_s + \alpha_1$ ,  $T = T_s + T_1$  and  $p = p_s + p_1$  with  $\underline{u}_1, \alpha_1, T_1, p_1 \ll 1$ . Linearizing (16)–(19) in the moving frame and utilizing (20) and (21) yields the evolution equations for the disturbances

$$\partial_z p_1 = -u_1 + \gamma_T T_1 - \alpha_1, \tag{25a}$$

$$\partial_y p_1 = -w_1, \tag{25b}$$

$$\partial_t \alpha_1 - c \partial_z \alpha_1 + u_1 d_z \alpha_s = \partial_z^2 \alpha_1 + \partial_y^2 \alpha_1 - Da f'(\alpha_s) \alpha_1, \tag{25c}$$

$$\begin{aligned} \partial_t T_1 - c \partial_z T_1 + u_1 d_z T_s = Le(\partial_z^2 T_1 + \partial_y^2 T_1) \\ + Da f'(\alpha_s) \alpha_1, \end{aligned} \tag{25d}$$

$$\nabla \cdot \underline{u}_1 = 0, \tag{25e}$$

where the prime indicates differentiation with respect to  $\alpha$ . We now seek solutions of (25) in the form of the normal modes

$$\begin{aligned} [u_1, w_1, p_1, \alpha_1, T_1] = [\bar{u}(z), \bar{w}(z), \bar{p}(z), \bar{\alpha}(z), \bar{T}(z)] \\ \times e^{\sigma t + iky} + \text{c.c.}, \end{aligned} \tag{26}$$

with  $\sigma$  the growth rate of the disturbances and  $k$  their wave-number. Substitution of (26) into (25) then yields

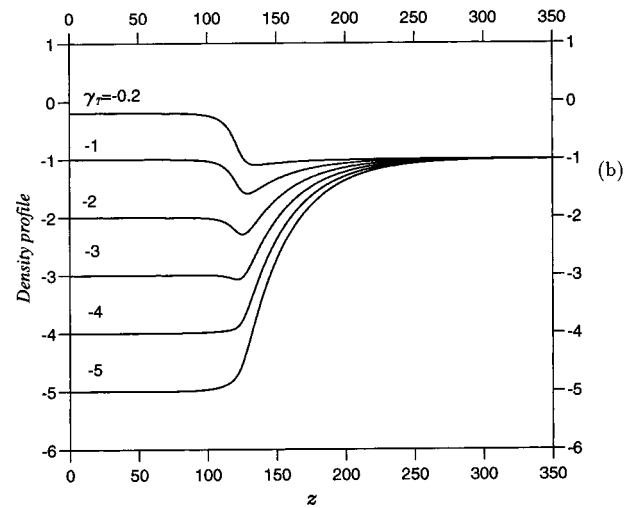
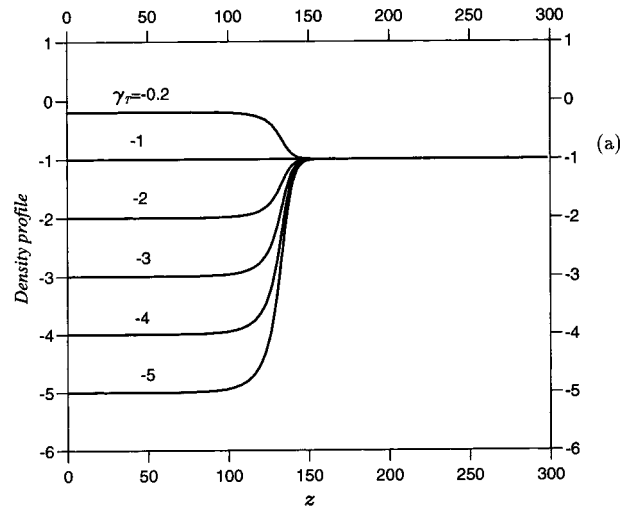


FIG. 4. Density contribution in Eq. (16),  $-\alpha + \gamma_T T$ , for two different values of the Lewis number.  $z=0$  corresponds to either the top or the bottom of the cell. In both cases the front propagates from the left to the right; (a)  $Le = 1$ ; (b)  $Le = 10$ .

$$d_z \bar{p} = -\bar{u} + \gamma_T \bar{T} - \bar{\alpha}, \tag{27a}$$

$$ik \bar{p} = -\bar{w}, \tag{27b}$$

$$\sigma \bar{\alpha} - cd_z \bar{\alpha} + \bar{u} d_z \alpha_s = d_z^2 \bar{\alpha} - k^2 \bar{\alpha} - Da f'(\alpha_s) \bar{\alpha}, \tag{27c}$$

$$\sigma \bar{T} - cd_z \bar{T} + \bar{u} d_z T_s = Le(d_z^2 \bar{T} - k^2 \bar{T}) + Da f'(\alpha_s) \bar{\alpha}, \tag{27d}$$

$$d_z \bar{u} + ik \bar{w} = 0. \tag{27e}$$

Differentiating now (27b) and (27e) once with respect to  $z$  gives  $d_z^2 \bar{u} + k^2 d_z \bar{p} = 0$  which when combined with (27a) results in

$$(d_z^2 - k^2) \bar{u} = -k^2 \gamma_T \bar{T} + k^2 \bar{\alpha}. \tag{28}$$

Equations (27c), (27d), and (28) can now be written as

$$\mathcal{L} \begin{bmatrix} \bar{\alpha} \\ \bar{T} \\ \bar{u} \end{bmatrix} = \sigma \begin{bmatrix} 1 & 0 & 0 \\ 0 & 1 & 0 \\ 0 & 0 & 0 \end{bmatrix} \begin{bmatrix} \bar{\alpha} \\ \bar{T} \\ \bar{u} \end{bmatrix}, \tag{29a}$$

where the elements of the matrix/differential operator  $\underline{\mathcal{L}}$  are given by

$$\begin{aligned} \mathcal{L}_{11} &= d_z^2 + cd_z - Daf'(\alpha_s) - k^2, \\ \mathcal{L}_{12} &= 0; \quad \mathcal{L}_{13} = -d_z\alpha_s; \quad \mathcal{L}_{21} = Daf'(\alpha_s), \\ \mathcal{L}_{22} &= Led_z^2 + cd_z - Lek^2; \quad \mathcal{L}_{23} = -d_zT_s, \\ \mathcal{L}_{31} &= -k^2; \quad \mathcal{L}_{32} = k^2\gamma_T; \quad \mathcal{L}_{33} = d_z^2 - k^2. \end{aligned}$$

The linear stability problem is hence governed by an infinite-domain generalized eigenvalue problem. The boundary conditions are

$$\bar{\alpha}, \bar{T}, \bar{u} \rightarrow 0 \quad \text{as } z \rightarrow \pm\infty, \tag{29b}$$

and, therefore, as with our previous study<sup>9</sup> we restrict our attention to the discrete spectrum of  $\underline{\mathcal{L}}$ , i.e., the spectrum consisting of eigenfunctions that decay to zero at the infinities and correspond to disturbances localized around the traveling front. We note, however, that infinite-domain eigenvalue problems might have an essential spectrum as well that consists of those eigenfunctions with bounded oscillatory behavior at the infinities (see, e.g., Refs. 31 and 32).

We solve the eigenvalue problem in (29) numerically by using a second-order central finite differencing scheme to approximate  $\underline{\mathcal{L}}$  with its discrete analog. The method is effectively the same with that used in our previous study:<sup>9</sup> We define  $\underline{U}$ ,  $\underline{A}$ , and  $\underline{T}$  as the discrete approximations of  $\bar{u}$ ,  $\bar{\alpha}$ , and  $\bar{T}$  and we invert the discrete representation of the operator  $d_z^2 - k^2$  in (28) to obtain an expression for  $\underline{U}$  as a function of  $\underline{A}$  and  $\underline{T}$  which when substituted in the discretized version of (27c) and (27d) yields a matrix eigenvalue problem of the form

$$\underline{M} \begin{bmatrix} \underline{A} \\ \underline{T} \end{bmatrix} = \sigma \begin{bmatrix} \underline{A} \\ \underline{T} \end{bmatrix}.$$

The LAPACK solver DGEEVX was then used to obtain the growth rate  $\sigma$  of the disturbances in the spanwise direction as a function of their wavenumber  $k$ . A large number of points in the integration domain was necessary for the first few eigenvalues with largest real parts to converge. We tested the accuracy of our scheme by varying the domain size and refining the mesh. Typical values for the domain size and mesh to achieve sufficient accuracy for the computation of the eigenvalues are 300 and 0.5, respectively.

### B. Dispersion curves and stability characteristics

We first discuss the up going front. Clearly, in the absence of thermal effects, the up going front is stable. Indeed, as the isothermal density increases in the course of the reaction, the reactants are lighter than the products and thus the solutal density stratification is buoyantly stable ( $\Delta\rho_S > 0$ ). However, for a nonzero reaction exothermicity, the products are hotter than the reactants, a thermally unstable stratification ( $\Delta\rho_T < 0$ ). For sufficiently large  $|\gamma_T|$ , the competition between stabilizing solutal stratification and unstable thermal stratification can give rise to an instability. Figure 5(a) depicts the least stable (largest) eigenvalue  $\sigma$  as a function of wavenumber  $k$  and different values of the modified thermal

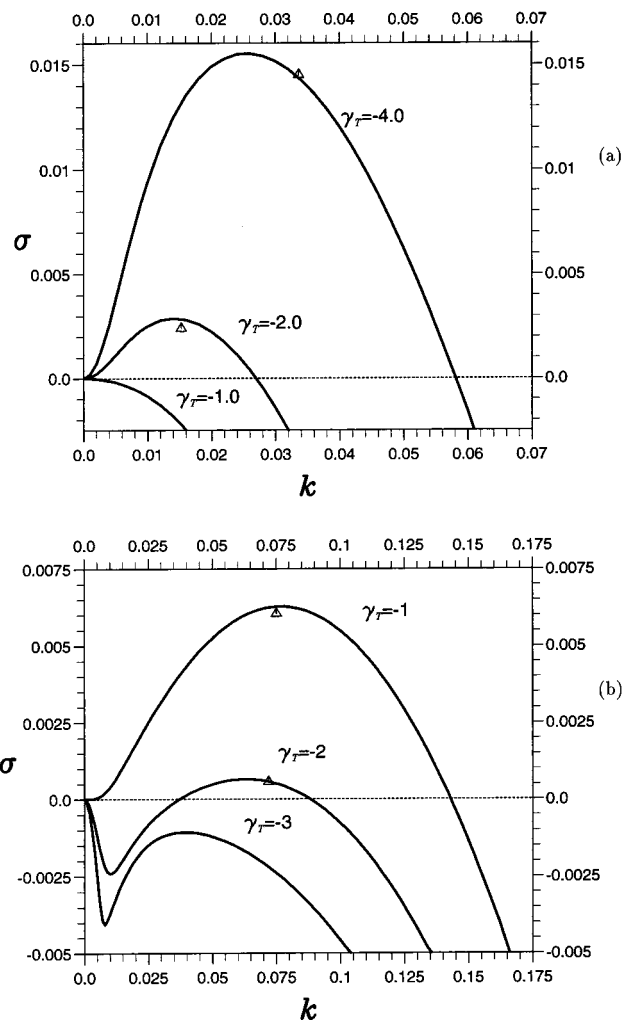


FIG. 5. Dispersion relation for the growth rate  $\sigma$  as a function of wavenumber  $k$  and different values of the modified thermal expansion coefficient  $\gamma_T$ . The triangles denote values of the most unstable wavenumber obtained at short times from the fully nonlinear system using as initial condition the traveling front or a step function; (a) up going front for  $Le = 10$ ; (b) down going front for  $Le = 4$ .

expansion coefficient  $\gamma_T$  for  $Le = 10$ . Notice that the translational invariance of the system in the streamwise direction implies that  $\sigma = 0$  for  $k = 0$ —this point was discussed in detail by Yang *et al.*<sup>9</sup>

Evidently, for a given  $Le$  there exists a critical value of  $|\gamma_T|$  above which the system becomes unstable. From the definition of  $\gamma_T$  in Sec. II, increasing  $|\gamma_T|$  can be achieved by either an increase of  $\phi$  and hence of the amount of heat released per mole of reactant and/or by an increase in  $\partial_T\rho$  which implies an increase in the density difference across the front for a given temperature gradient.

Note that the dispersion curves of the upgoing front always feature a band of unstable modes extending from zero wavenumber up to a cut-off wavenumber above which the system is linearly stable. This unstable band  $0 \leq k \leq k_c$  contains the maximum growing wavenumber  $k_{\max}$  with the largest positive growth rate. Such curves are similar to those obtained in standard Rayleigh–Taylor fingering (see, for example, Refs. 33 and 34). According also to the classification

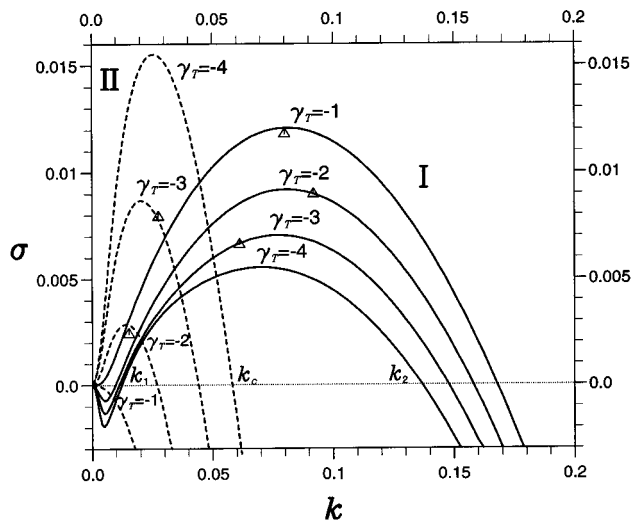


FIG. 6. Dispersion curves for both up going (dashed lines) and down going fronts (solid lines) for  $Le=10$  and  $\gamma_T = -4, -3, -2, -1$ . Type I dispersion curves have a band of unstable modes such that  $k_1 \leq k \leq k_2$  while type II dispersion curves have modes with positive growth rates in the range  $0 \leq k \leq k_c$ .

by Cross and Hohenberg,<sup>35</sup> such dispersion curves are of type II.

Solutal and thermal effects compete the other way round for the downward moving front. Figure 5(b) shows the dispersion curves for  $Le=4$  and different values of  $\gamma_T$ . In the absence of thermal effects ( $\gamma_T=0$ ) now, the denser products lie on top of the lighter reactants and the front is buoyantly unstable because of unfavorable solutal stratification as studied by Yang *et al.*<sup>9</sup> This solutal destabilization in the absence of heat effects is characterized by dispersion curves which are similar to those found in standard Rayleigh–Taylor fingering, i.e., they feature a band of unstable modes from  $k=0$  to a cut-off wavenumber  $k_c$ .

Heat effects now have a stabilizing influence as the “hot” products lie on top of the “cold” reactants, a stable configuration. Therefore, the competition between thermal and solutal effects here is opposite to that of the upgoing front. If heat effects are strong, the solutal fingering of the down going front should be stable. Indeed, we observe that for large  $|\gamma_T|$ , the growth rate is always negative implying that strongly exothermic down going fronts are propagating without any fingering. There exists, however, a critical value of  $|\gamma_T|$  below which competition between the solutal and thermal effects drastically changes the dispersion curves leading to stabilization of long waves and destabilization of a band of wavenumbers centered around a most unstable mode  $k_{\max}$  and bounded by two neutral wavenumbers  $k_1$  and  $k_2$  such that  $0 < k_1 \leq k \leq k_2$ . Such dispersion curves are of type I<sup>35</sup> (but with a neutral mode always at zero wavenumber) and are also reminiscent of Turing-type dispersion curves.<sup>36–38</sup> Figure 5(b) then shows that decreasing  $|\gamma_T|$  can lead from stable fronts to Turing-type and finally to standard Rayleigh–Taylor fingering dispersion curves.

To summarize the differences between the stability properties for the up and down going fronts, let us look at Fig. 6 which compares the dispersion curves of the two counter-

propagating fronts for  $Le=10$  and four different values of  $\gamma_T$ . For  $\gamma_T = -4, -3, -2$ , both fronts are simultaneously unstable but with different maximum growing wavenumbers and growth rates. The most unstable wavenumber for the downgoing front (reaction triggered at the top) is larger than that of the upgoing front (reaction triggered at the bottom). This implies that the wavelength of the developed fingers for the up going front will be much larger than that of the down going front. In addition, the down going front features a band of stable modes close to  $k=0$  which is reminiscent of Turing-type dispersion curves. This implies a long term dynamics of the down going front quite different from that of the up going front as will be shown in the next section. Note also that for  $\gamma_T = -4, -3$  the growth rate of the up going front is larger than that of the down going front which means that the up going front will be the first to become unstable and show fingering. For smaller  $|\gamma_T|$ , the reverse is observed, now it is the down going front that will finger first. These theoretical predictions are in agreement with the recent experiments by Bánsági *et al.*<sup>29</sup> which confirm the type I dispersion curves for the down going front.

Let us now return to the density profiles in Fig. 4(b). These profiles indicate that as  $|\gamma_T|$  increases the downward front should become more stable since the total density of the products becomes smaller than the density of the reactants. For the same reason, the up going front should become increasingly unstable. This general trend is consistent with the findings of our linear stability analysis. Notice, however, that for  $\gamma_T = -4, -3, -2$ , and  $-1$ , Fig. 6 indicates that the down going front is unstable even though from the density plots in Fig. 4(b) we clearly have a light fluid on top of a heavy fluid for  $\gamma_T = -4, -3, -2$  and two fluids of the same density for  $\gamma_T = -1$ .

Of course for some values of  $\gamma_T$  the density profiles are nonmonotonic and in fact they have a minimum around the front, a potentially unstable situation for the down going front. However, for  $\gamma_T = -3$  the minimum of the density profile is very small and hence nonmonotonic density cannot account for the apparent contradiction between Figs. 4(b) and 6. In fact, for  $\gamma_T = -4$  the density profile is monotonic with a light fluid on top of a heavy fluid and yet our linear stability analysis clearly shows that the down going front is linearly unstable (evidently a light fluid on top of a heavy fluid should always be a stable configuration in the absence of disturbances; it is the linear stability analysis that examines the response of the system to small perturbations that uncovers the instability when, e.g.,  $Le=10$  and  $\gamma_T = -4$ ). On the other hand for  $Le=1$  [see Fig. 4(a) for the density profiles] the stability results are as expected, i.e., light fluid on top of heavy fluid is a stable configuration while heavy fluid on top of light fluid leads to an instability.

This then suggests that the instability mechanism entails double-diffusive convection phenomena. A classical example of such phenomena is the so-called “thermohaline convection” or “salt fingers” which arise when hot saline water lies on top of cold fresh water.<sup>17,18</sup> This instability is due to the very different rates of diffusion of heat and salt (heat diffuses faster than mass). This is just one example of a more general situation, for instance one might have no temperature varia-



TABLE I. Stability characteristics of the down going front as a function of  $Le$  and  $\gamma_T$ . Stable configurations are denoted by S and unstable ones by U.

$\gamma_T$	$Le$	Linear stability result	
-0.2	1.0	U	
	-1.0	1.0	S
		2.0	U
		1.0	S
		2.0	S
-2.0	3.0	S	
	4.0	S	
	4.5	U	
	-3.0	1.0	S
		2.0	S
3.0		S	
-4.0	4.0	S	
	4.5	S	
	5.0	U	
	-1.0	1.0	S
		2.0	S
3.0		S	
4.0		S	
5.5		U	

tions but two different solutes with different diffusivities. In the context of reaction–diffusion systems, the significance of double-diffusive convection phenomena was first suggested by Pojman and co-workers.<sup>3,10</sup> The emphasis of these studies was on the effect of double-diffusion convection on the propagation velocity of the fronts. These authors used qualitative arguments to explain the influence of convective effects on front propagation for the Belousov–Zhabotinskii and iron(II)-nitric acid systems in narrow tubes without any quantitative modeling of the experiments.

The trend in Fig. 6 now indicates that for  $Le = 10$  and some large negative value of  $\gamma_T$ , the down going front should be stable, as expected. The fundamental question then is why, e.g., when  $Le = 10$  and  $\gamma_T = -4$  the down going front is unstable while for the same value of the Lewis number and a higher negative value of the expansion coefficient, e.g.,  $\gamma_T = -6$  the down going front is found to be stable. After all in both cases we have a light fluid on top of a heavy fluid.

For a given Lewis number  $Le > 1$ , heat diffuses faster than mass and the hot products will lose their heat to the cold reactants. This fast diffusion of heat can cool the products sufficiently so that they become heavier than the reactants which leads to an instability. Of course heat is produced continuously by the reaction, but at the same time, provided that the reaction exothermicity  $\phi$  is small (recall that  $\gamma_T = \phi\Gamma_T$ ), thermal diffusion can transport the heat to the reactants thus cooling the products sufficiently which can then become heavier than the reactants. If on the other hand  $\phi$  is large, thermal diffusion cannot remove the heat of the products sufficiently fast (there is simply too much heat in the products). In this case we have a stable configuration.

The above of course depends on the Lewis number. Evidently, as the Lewis number increases, the value of  $\phi$  and hence  $|\gamma_T|$  above which the down going front is stabilized must increase to compensate for the increasingly fast diffusion of heat. Table I summarizes the stability properties of

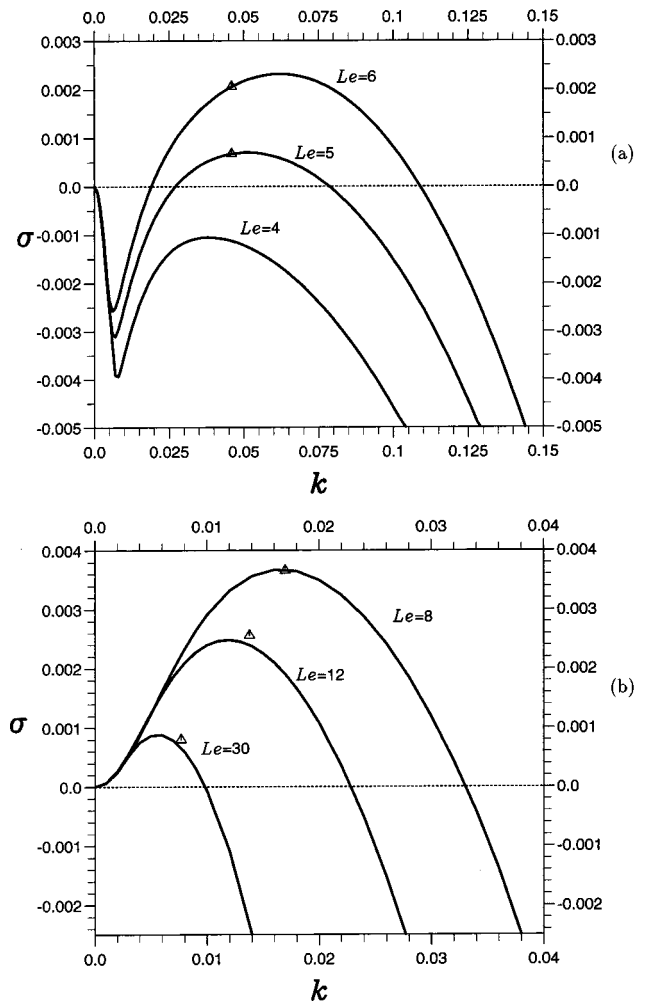


FIG. 7. Effect of Lewis number on the dispersion curves; (a) down going fronts for  $\gamma_T = -3$  and three different values of  $Le$ ; there is a critical Lewis number between 4 and 5 for the given parameters below which the system is stable; (b) up going fronts for  $\gamma_T = -2$  and three different values of  $Le$ . The triangles are the values of the most unstable wavenumber observed at short times in the fully nonlinear system using as initial condition the traveling front or a step function.

the down going front in the  $\gamma_T$ – $Le$  plane. The table gives only the approximate stability map in this plane and for a more accurate prediction of the critical Lewis number  $Le_{crit}$  above which the down going front loses stability, a smaller mesh for  $Le$  is required. Nevertheless, the table indicates that  $Le_{crit}$  increases as  $|\gamma_T|$  increases. This general trend is consistent with our observation that as  $\phi$  increases (hence  $|\gamma_T|$  increases)  $Le$  must increase to compensate for the large amount of heat in the products and cause a double diffusion instability.

For a given  $\gamma_T$ , therefore, the down going front is becoming increasingly unstable as  $Le$  increases. This is consistent with Fig. 7(a) which shows the dispersion curves of the down going front for  $\gamma_T = -3$  and three values of  $Le$ . For the up going front the Lewis number has the opposite effect so that increasing  $Le$  makes the system more stable [see Fig. 7(b)]. This is due to the fact that double-diffusive convection acts differently for the up going and down going fronts. In fact, for the down going front double-diffusive convection

has a destabilizing influence so that increasing  $Le$  makes the down going front more unstable. The up going front, however, is stable with respect to double-diffusive convection. Indeed, heat now diffuses from the hot products to the cold reactants thus making the products cooler and hence heavier. This effect is obviously amplified as  $Le$  increases.

Notice here that for the down going front our computations show that whenever the corresponding density profile indicates that the front should be stable but our linear stability analysis shows that it is unstable, the instability is characterized by type I (or Turing-type) dispersion curves. A typical example is the case  $Le=10$  and  $\gamma_T=-4$  we discussed above. This then suggests that the dispersion curves in this case result from the competition between two factors: buoyancy which is stabilizing and is trying to bring down  $\sigma$  towards negative values and double-diffusive convection which is destabilizing and is trying to increase  $\sigma$  towards positive values.

We should also point out that it is impossible to isolate the effect of the nonmonotonic density profiles on the stability characteristics although clearly they do play a role. In the absence of double-diffusive convection, i.e., for  $Le=1$ , the density profile is always monotonic. Nonmonotonic density requires  $Le>1$  in which case double-diffusive convection is also present. On the other hand, for certain values of  $Le$  and  $\gamma_T$ , e.g.,  $Le=10$  and  $\gamma_T=-4$  the density profile is monotonic and yet the down going front is found to be unstable. Hence the situation here is different to the viscous fingering problem with nonmonotonic viscosity profiles and without any chemical reactions investigated by Manickam and Homsy<sup>39–41</sup> where the effect of the viscosity nonmonotonicity was clearly identified and quantified (viscosity nonmonotonicity was found to be responsible for new phenomena referred to by the authors as “reverse fingering”).

We close this section with a comment on the mechanism of the instability. As we already pointed out, for  $Le=1$  there is no double-diffusion convection. In this case the instability results from a competition between solutal and thermal effects through the kinetic term  $f(\alpha)$  and the buoyancy term  $\gamma_T T - \alpha$  (the chemistry increases  $T$  which then decreases  $\rho$ ). For  $Le>1$  double-diffusion convection is also present and the instability now results from a complex interplay between solutal/thermal effects, chemical reaction and double-diffusive phenomena. Hence, due to the presence of the chemical reaction, the instability mechanism is quite different to pure double diffusion where only two competing factors are present (diffusion and heat effects). In addition, in simple double diffusion, the basic concentration and temperature profiles prior to the instability, are externally imposed and in general they vary linearly in space *independently* of the Lewis number. For chemical fronts, it is the coupling between the kinetics and diffusion that provides the concentration and temperature profiles. The base state (in the form of traveling fronts) is therefore a function of the Lewis number itself which makes the interplay between mass and temperature gradients much more subtle than in standard double diffusion.

## V. NONLINEAR DYNAMICS

To analyze the nonlinear stage of the instability and to get insight into the long term dynamics of the developed fingers, we consider the fully nonlinear system in Eqs. (16)–(19). Introducing the stream function  $\psi$  such that  $u = \partial_y \psi$  and  $w = -\partial_x \psi$  with  $\underline{u} = u\hat{i}_x + w\hat{i}_y$ , and taking the curl of the evolution equation for the pressure distribution (16) yields

$$\partial_x^2 \psi + \partial_y^2 \psi = -\partial_y \alpha + \gamma_T \partial_y T, \quad (30)$$

$$\partial_t \alpha + \partial_x \alpha \partial_y \psi - \partial_y \alpha \partial_x \psi = \partial_x^2 \alpha + \partial_y^2 \alpha - 36Da\alpha \times (1-\alpha)^2 (\kappa + 7\alpha), \quad (31)$$

$$\partial_t T + \partial_x T \partial_y \psi - \partial_y T \partial_x \psi = Le(\partial_x^2 T + \partial_y^2 T) + 36Da\alpha \times (1-\alpha)^2 (\kappa + 7\alpha). \quad (32)$$

We numerically solve Eqs. (30)–(32) using a pseudo-spectral method in a two-dimensional domain of dimensionless width  $L_y$  and length  $L_x$ . The numerical scheme is essentially the same as that described in Refs. 9, 28, and 42 and is based on Fourier expansions for the stream function  $\psi$ , concentration  $\alpha$  and temperature  $T$  and hence, periodic boundary conditions are imposed in both the transverse and streamwise directions. We derive a set of ordinary differential equations for the evolution of the time-dependent coefficients of the Fourier expansions. These equations are solved numerically using a second-order Adams–Bashforth scheme. The initial condition is taken as a step function, i.e., the flat front profile switching close to the upper boundary of the system from the stable steady state  $\alpha=0, T=1$  (in white color on the density plots to be presented) to the unstable steady state  $\alpha=1, T=0$  (in black). The reverse switch is imposed close to the bottom of the system. This allows us to deal with the periodicity in the  $x$ -direction. Alternatively, the initial condition can be taken as the planar front constructed numerically in Sec. III and located close to the upper and lower boundaries of the system. As the stable steady state invades the unstable steady state, the upper front will move downwards leaving hotter but heavier (white) products on top of the colder but lighter fresh reactants (in black) while the lower front will move upwards leading to a stratification of cold, lighter reactants on top of hotter but heavier products. Depending on the relative strength of solutal and thermal effects, fingering of either one or both fronts is observed.

To compare our nonlinear simulations to the linear stability analysis of the previous section, we measure the maximum growth rate and most unstable wavelength. The growth rate is obtained by fitting an exponential to the evolution of the length of the fingers as a function of time for small times. To obtain the wavelength of the developed fingers we take the power spectrum of the front at early times. The wavelength is in excellent agreement with the values predicted by the linear stability analysis. Figures 5 and 7 compare the linear stability analysis with the fully nonlinear simulations and in all cases the agreement is very good. The results are roughly the same whether the initial condition is the traveling front solution or a step function.

We now focus on the nonlinear stage of the instability. Figure 8 shows a typical example of the spatio-temporal be-

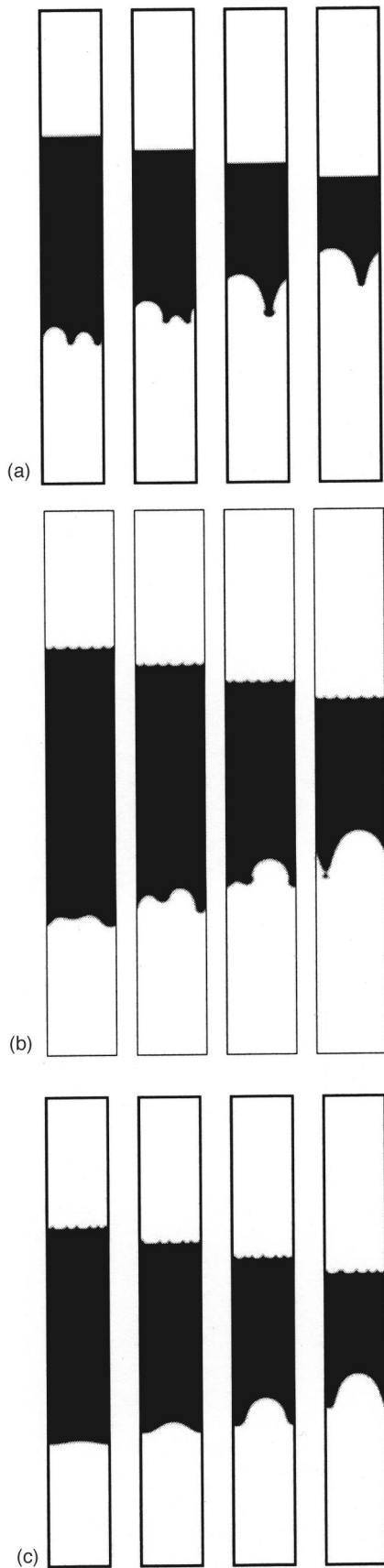


FIG. 8. Nonlinear dynamics of buoyantly unstable exothermic CT fronts with  $\gamma_T = -2$  and four successive times from left to right. In all our numerical experiments the system size is  $L_y = 512$ ,  $L_x = 4096$ ; (a)  $Le = 4$ ; (b)  $Le = 6$ ; (c)  $Le = 8$ .

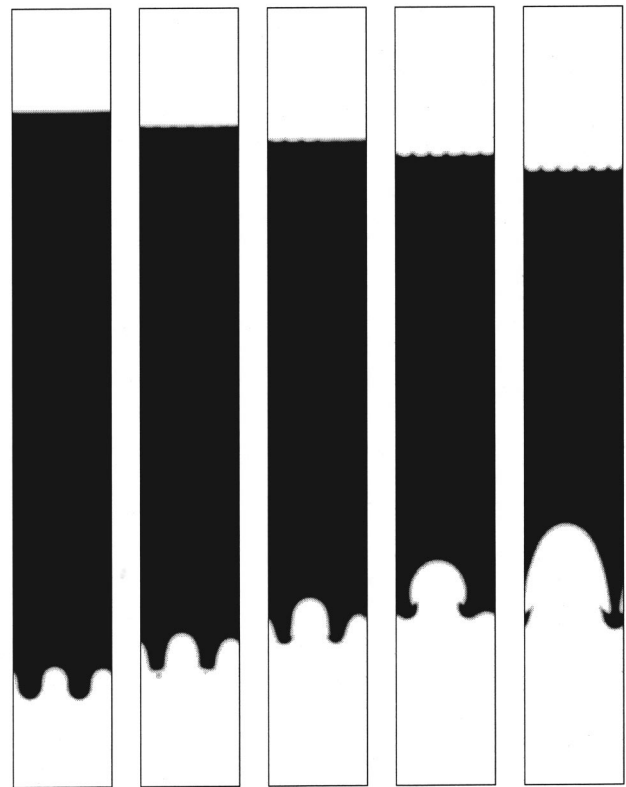


FIG. 9. Nonlinear dynamics for  $\gamma_T = -3$  and  $Le = 8$ , at successive times from left to right. The up going front features mushrooms and coarsening typical of type II dispersion curves. The down going front develops fingers of constant amplitude and wavelength. Their small amplitude results from small growth rates for these values of the parameters.

havior of the fully nonlinear system when two counterpropagating fronts are initiated at the top and bottom of the cell. The simulations are obtained using  $\gamma_T = -2$  and three different values of the Lewis number,  $Le = 4, 6$ , and  $8$ . In all our nonlinear simulations the domain size is fixed at  $L_y = 512$  and  $L_x = 4096$ . For  $Le = 4$  only the up going front is unstable featuring initially two big fingers that merge into one single finger of constant shape and speed. Its velocity is larger than the speed of the flat front as convection is entraining the front.<sup>1-3,28</sup> Increasing the Lewis number, stabilizes the up going front and destabilizes the down going front, in agreement with our discussion in the previous section. For the up going fronts for instance, fingers appear at larger times and with a larger wavelength (i.e., smaller most unstable wave-number) as  $Le$  increases. For  $Le = 6$ , the growth rates of the two fronts are of the same order of magnitude and hence fingering appears on both fronts roughly at the same time. The lower front still presents two fingers that will ultimately merge into a single finger. This lonely finger has nevertheless a smaller mixing zone and smaller speed as now the extension of the convection roll is smaller. For higher exothermicities and higher Lewis numbers, the up going front features thermal plumes of mushroom shape (see, for example, Fig. 9). Nevertheless, one always ends up with one single finger traveling with constant shape. This is typical of standard Rayleigh–Taylor fingering dispersion curves (or type II) for which all modes from  $k = 0$  until  $k = k_c$  are unstable. In

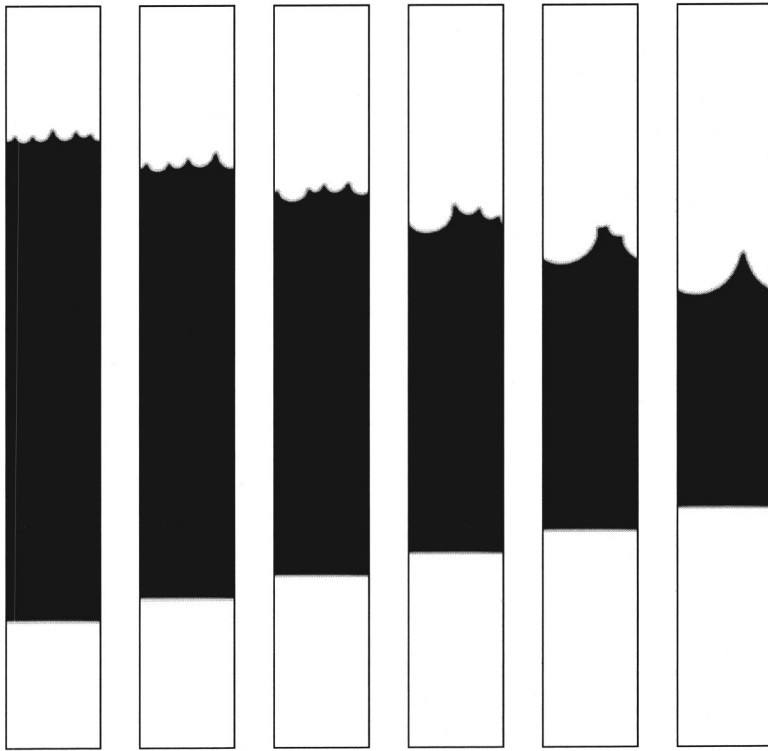


FIG. 10. Nonlinear dynamics of a down going front characterized by type II dispersion curve as in standard Rayleigh–Taylor fingering. The parameters are  $\gamma_T = -0.5$  and  $Le = 2$ .

this case, the wavelength at onset is given by  $\lambda = 2\pi/k_{\max}$  measured between subsequent tips and the resulting fingering pattern has an amplitude, i.e., a distance between subsequent tips and troughs of the fingered zone, which grows in time. The nonlinear stage of the instability is characterized by coarsening of the fingers in the course of time due to merging and shielding phenomena.<sup>28,43</sup>

The upper front also features fingering but of much smaller amplitude and wavelength. Interestingly, no coarsening is observed and the wavelength as well as mixing zone remain constant in time. In fact the system evolves to a stationary cellular structure of wavenumber  $k_{\max}$  as in the case of Turing patterns<sup>35–38</sup> or Rayleigh–Bénard convection.<sup>44</sup> Whenever a stationary pattern is observed in our computations, the corresponding dispersion curves are of the Turing-type or type I. It is well known that such dispersion curves are characterized by a critical value of a control parameter (e.g.,  $\gamma_T$  for the curves in Fig. 6) at which the base state undergoes a stationary instability.<sup>35</sup> However, linear stability alone cannot determine the long-time behavior of the system and such curves do not necessarily imply equilibrated, finite amplitude fronts away from criticality and at the nonlinear stage of the instability. Indeed, there are several systems, e.g., channel flow and Blasius boundary layer<sup>45</sup> with type I dispersion curves which do not equilibrate to stationary norm solutions. The issue of whether or not the instability equilibrates to a stationary norm state is essentially a nonlinear question. Our computations of the fully nonlinear system show that indeed the instability of the down going front saturates leading to a stationary norm pattern whenever the dispersion curves are of type I. The instability simply cannot propagate indefinitely because it encounters the thermal sta-

bilizing effect. We note here that such changes from type II to type I dispersion curves have also been obtained in the context of density/viscous fingering in the absence of chemical reactions by Manickam and Homsy,<sup>41</sup> without, however, stationary patterns. To our knowledge, the stationary patterns obtained here have not been observed before in the context of fingering instabilities.

Notice that the small amplitude of the stationary pattern in Figs. 8 and 9 results from small growth rates for the values of the parameters used here. It is also important to point out that for type I dispersion curves, weakly nonlinear theories can be pivoted about the degree of supercriticality and about the mode with  $k_{\max}$  at criticality to obtain Ginzburg–Landau-type equations<sup>35,38,44</sup> in this region. Such weakly nonlinear analyses, however, are beyond the scope of the present study.

For  $Le = 8$  and  $\gamma_T = -2$  [see Fig. 8(c)], the upper front is the first one to become unstable. The mixing zone remains constant in time but the system is here further away from criticality and the band of unstable modes is now much larger. This leads to a nonlinear dynamics which is much more complex as birth and death of fingers is continuously observed, the number of fingers varying between 5 and 6 in the course of time.

For down going fronts, the dispersion curves can be of standard Rayleigh–Taylor fingering-type or Turing-type depending on the values of parameters [see, e.g., Fig. 5(b)]. Figure 10 depicts the nonlinear dynamics of a down going front for  $Le = 2$  and  $\gamma_T = -0.5$  for which the dispersion curve is of type II as in standard Rayleigh–Taylor fingering. Just as for other up and down going fronts in the absence of heat effects (see, e.g., Refs. 9 and 28), coarsening of the fingers is eventually observed and one single final finger of



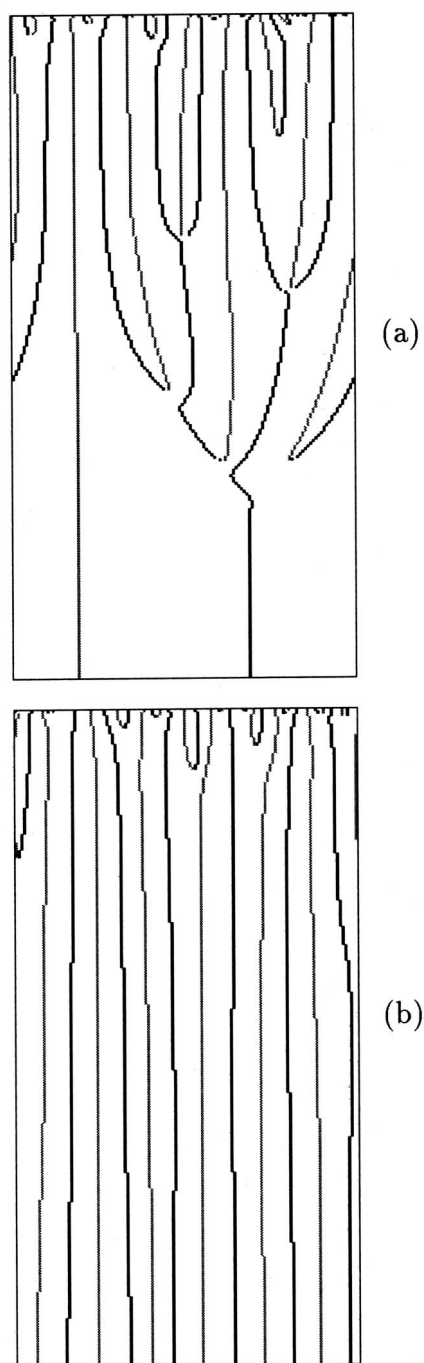


FIG. 11. Space–time map of the position of the maxima (black curves) and minima (gray curves) of the fingers for the down going front; (a)  $Le=2$  and  $\gamma_T=-0.5$  (type II dispersion curves); (b)  $Le=5$  and  $\gamma_T=-2.0$  (Turing/type I dispersion curves). These positions are determined from the averaged profile of the upper half of the system obtained by integrating along the  $x$ -direction. The horizontal axis corresponds to the width of the system ranging from 0 to  $L_y$ , while time increases from top to bottom.

constant shape and speed is the asymptotic dynamics for large times. To characterize this coarsening dynamics, we plot in Fig. 11 the positions of the maxima and minima of the longitudinally averaged profile as a function of time. It is clearly seen that the number of fingers diminishes in the course of time so that starting with roughly 13 fingers at short times, fingers merge leading to an overall coarsening

and finally we end up with one single lonely finger [Fig. 11(a)]. This is to be contrasted with the dynamics of a Turing-type dispersion curve shown in Fig. 11(b) obtained for  $Le=5$  and  $\gamma_T=-2$ . In this case, the system maintains six fingers all along and the mixing zone remains constant as well. A comparison between the coarsening of Fig. 11(a) and the fixed wavenumber patterning of Fig. 11(b) is further seen on Fig. 12 which compares the modes of maximum power in the Fourier transform of the longitudinally averaged profile as a function of time. When the dispersion curve is of standard Rayleigh–Taylor fingering-type, fairly quickly the mode with the highest power corresponds to  $n=1$  which means that the system evolves towards a situation with one single finger across the width of the Hele–Shaw cell. On the contrary, for the Turing-type dispersion curve, the mode with highest power remains at  $n=6$  which means that the system maintains six fingers all along. Notice that an extensive parametric study of the nonlinear stage of the instability (as well as the linear stage examined in the previous section) for a large variety of the governing dimensionless groups has been performed by Yang.<sup>46</sup>

Finally, it is important to point out that for standard Rayleigh–Taylor instabilities of nonreactive fluids, it is known that fingering leads to fingers which grow continuously in time so that their mixing zone increases monotonically in time.<sup>34,47</sup> It has been shown in detail previously, both for monostable<sup>28</sup> and bistable kinetics<sup>48</sup> and is further evidenced here, that the presence of a chemical reaction drastically changes this nonlinear dynamics. Indeed, coarsening towards one single finger is observed for monostable kinetics while droplet formation is observed for bistable ones. It is thus not surprising that chemical reactions also drastically modify the nonlinear dynamics of the double-diffusive instability. Standard “salt fingers” observed for opposite concentration and thermal gradients for  $Le>1$ ,<sup>17,18</sup> are typically thin localized fingers that stretch continuously in time. In contrast with these well studied nonreactive salt fingers, double diffusion of chemical fronts features “frozen” small fingers of constant amplitude and mixing zone, which demonstrates once again, the significant influence of chemical reactions on hydrodynamic instabilities.

## VI. DISCUSSION

We have examined in detail the density fingering of exothermic reaction-diffusion fronts in Hele–Shaw cells using the CT reaction as a model system. In particular, we focused on the influence of heat effects on the stability properties and nonlinear dynamics of the resulting fingering instabilities. We analyzed here the case where thermal and solutal contributions to the density jump across the front are of opposite signs ( $\Delta\rho_S>0, \Delta\rho_T<0$ ). The governing equations were derived using the Darcy–Boussinesq approximation. We constructed the minimum speed concentration and temperature fronts and we performed a linear stability analysis of these fronts with respect to infinitesimal disturbances in the spanwise direction. For the ascending fronts the dispersion curves are similar to those observed in standard Rayleigh–Taylor fingering. The descending fronts on the other hand can fea-

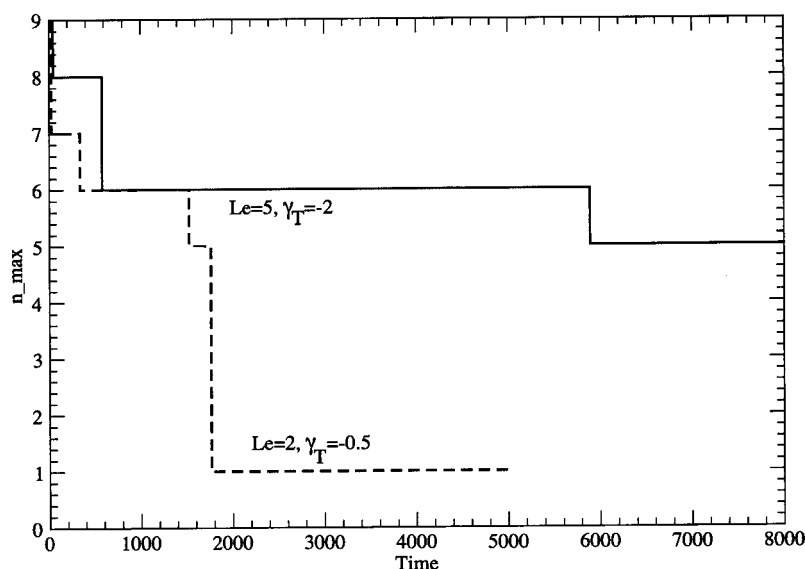


FIG. 12. Mode of highest power as a function of time for the two simulations of Fig. 11.

ture dispersion curves of the Turing type. We analyzed the stability properties of both descending and ascending fronts and showed that the instability is due to a complex interplay between solutal–thermal effects, chemical reaction and double-diffusive phenomena (which play a role only for a Lewis number larger than unity). These results enlighten recent experimental observations of Turing-type dispersion curves for descending fronts in the chlorite–tetrathionate reaction.<sup>29</sup>

We then analyzed the nonlinear stage of the instability by performing numerical experiments from the fully nonlinear system. At the onset of the fingering instability, our time-dependent computations were found to be in excellent agreement with the predictions of the linear stability analysis. At the nonlinear stage of the instability up going fronts feature thermal plumes of mushroom shape while coarsening of the developed fingers in the course of time due to merging and shielding phenomena was observed. As a result of this coarsening process, all fingers merge into a single finger for large times. Down going fronts on the other hand, can behave dramatically differently. We have provided here evidence of a new type of fingering phenomenon resulting from the coupling between solutal and thermal effects: Depending on the values of the relevant dimensionless groups, down going fronts can feature stationary norm cellular states with fingers of constant amplitude and wavelength.

The present work suggests several further studies and directions. First of all, we have used here the two-dimensional (2D) Darcy equation to model the flow in a Hele-Shaw cell or a porous medium. This demonstrates that the new fingering phenomena and new type of dispersion curves analyzed in the present study, result genuinely from 2D dynamics due to the complex interplay between chemistry, heat effects and hydrodynamics. They should be observed experimentally using exothermic reactions in Hele-Shaw cells with very thin gapwidths. It would be instructive to analyze the same systems for larger gapwidths using two-dimensional Navier–Stokes–Darcy (NSD) or three-dimensional (3D) Stokes equations along the lines of other

authors<sup>49–52</sup> to assess the influence of 3D effects.

Finally, it has been shown recently that for systems of small lateral extent, density fingering of monostable isothermal chemical fronts leads to one single self-similar finger while for larger systems, tip splittings are observed.<sup>28</sup> The single final finger follows interesting scaling laws. Obviously, as shown here, such single fingers are obtained also for exothermic reactions in some regions of the parameter space. It would be of interest to analyze to what extent heat effects modify the scaling laws of the isothermal self-similar fingers as well as the occurrence of tip splittings for larger systems.

## ACKNOWLEDGMENTS

We are grateful to G. M. Homsy for helpful comments and suggestions. We also acknowledge fruitful discussions with A. Zebib, D. Horváth, and A. Tóth. This work was supported by the University of Leeds through an ORS award, an EPSRC Advanced Research Fellowship, the ESF Reactor Program, ESA, Prodex and FRFC (Belgium). A.D. is Research Associate of the FNRS (Belgium).

<sup>1</sup>G. Bazsa and I. Epstein, “Traveling fronts in the nitric acid–iron(II) reaction,” *J. Phys. Chem.* **89**, 3050 (1985).

<sup>2</sup>I. Nagypál, G. Bazsa, and I. Epstein, “Gravity-induced anisotropies in chemical fronts,” *J. Am. Chem. Soc.* **108**, 3635 (1986).

<sup>3</sup>J. A. Pojman and I. Epstein, “Convective effects on chemical fronts. 1. Mechanisms and stability criteria,” *J. Phys. Chem.* **94**, 4966 (1990).

<sup>4</sup>J. A. Pojman, I. Epstein, T. McManus, and K. Showalter, “Convective effects on chemical fronts. 2. Simple convection in the iodate–arsenous acid system,” *J. Phys. Chem.* **95**, 1299 (1991).

<sup>5</sup>J. Masere, D. Vasquez, B. Edwards, J. Wilder, and K. Showalter, “Non-axisymmetric and axisymmetric convection in propagating reaction–diffusion fronts,” *J. Phys. Chem.* **98**, 6505 (1994).

<sup>6</sup>M. Carey, S. Morris, and P. Kolodner, “Convective fingering of an autocatalytic reaction front,” *Phys. Rev. E* **53**, 6012 (1996).

<sup>7</sup>M. Böckmann and S. C. Müller, “Growth rates of the buoyancy-driven instability of an autocatalytic reaction front in a narrow cell,” *Phys. Rev. Lett.* **85**, 2506 (2000).

<sup>8</sup>D. Horváth, T. Bánsági, Jr., and Á. Tóth, “Orientation-dependent density fingering in an acidity front,” *J. Chem. Phys.* **117**, 4399 (2002).

<sup>9</sup>J. Yang, A. D’Onofrio, S. Kalliadasis, and A. De Wit, “Rayleigh–Taylor

- instability of reaction–diffusion acidity fronts,” *J. Chem. Phys.* **117**, 9395 (2002).
- <sup>10</sup>J. A. Pojman, I. Nagy, and I. Epstein, “Convective effects on chemical fronts. 3. Multicomponent convection in the iron(II)–nitric acid system,” *J. Phys. Chem.* **95**, 1306 (1991).
- <sup>11</sup>I. Nagy and J. A. Pojman, “Multicomponent convection induced by fronts in the chlorate–sulfite reaction,” *J. Phys. Chem.* **97**, 3443 (1993).
- <sup>12</sup>C. Chinake and R. Simoyi, “Fingering patterns and other interesting dynamics in the chemical fronts generated by the chlorite–thiourea reaction,” *J. Phys. Chem.* **98**, 4012 (1994).
- <sup>13</sup>A. Keresztessy, I. Nagy, G. Bazsa, and J. A. Pojman, “Traveling fronts in the iodate–sulfite and bromate–sulfite systems,” *J. Phys. Chem.* **99**, 5379 (1995).
- <sup>14</sup>A. Komlósi, I. Nagy, G. Bazsa, and J. A. Pojman, “Convective chemical fronts in the 1,4-cyclohexanedione-bromate-sulfuric acid-ferroin system,” *J. Phys. Chem.* **102**, 9136 (1998).
- <sup>15</sup>J. A. Pojman, R. Craven, A. Khan, and W. West, “Convective instabilities in traveling fronts of addition polymerization,” *J. Phys. Chem.* **96**, 7466 (1992).
- <sup>16</sup>M. Belk, K. G. Kostarev, V. Volpert and T. M. Yudina, “Frontal photopolymerization with convection,” *J. Phys. Chem. B* **107**, 10292 (2003).
- <sup>17</sup>J. S. Turner, “Multicomponent convection,” *Annu. Rev. Fluid Mech.* **17**, 11 (1985).
- <sup>18</sup>D. J. Tritton, *Physical Fluid Dynamics* (Oxford University Press, 1988).
- <sup>19</sup>B. Edwards, J. Wilder, and K. Showalter, “Onset of convection for autocatalytic reaction fronts: Laterally unbounded system,” *Phys. Rev. A* **43**, 749 (1991).
- <sup>20</sup>D. Vasquez, B. Edwards, and J. Wilder, “Onset of convection for autocatalytic reaction fronts: Laterally bounded systems,” *Phys. Rev. A* **43**, 6694 (1991).
- <sup>21</sup>J. Wilder, B. Edwards, and D. Vasquez, “Finite thermal diffusivity at onset of convection in autocatalytic systems: Continuous fluid density,” *Phys. Rev. A* **45**, 2320 (1992).
- <sup>22</sup>D. Vasquez, B. Edwards, and J. Wilder, “Finite thermal diffusivity at onset of convection in autocatalytic systems: Discontinuous fluid density,” *Phys. Fluids* **7**, 2513 (1995).
- <sup>23</sup>D. Vasquez, J. Wilder, and B. Edwards, “Convective instability of autocatalytic reaction fronts in vertical cylinders,” *Phys. Fluids A* **4**, 2410 (1992).
- <sup>24</sup>B. McCaughey, J. A. Pojman, C. Simmons, and V. Volpert, “The effect of convection on a propagating front with a liquid product: Comparison of theory and experiments,” *Chaos* **8**, 520 (1998).
- <sup>25</sup>M. Garbey, A. Täik, and V. Volpert, “Influence of natural convection on stability of reaction fronts in liquids,” *Q. Appl. Math.* **56**, 1 (1998).
- <sup>26</sup>D. Zhang, W. Peltier, and R. Armstrong, “Buoyant convection in the Belousov–Zhabotinsky reaction. II. Chemically driven convection and instability of the front structure,” *J. Chem. Phys.* **103**, 4078 (1995).
- <sup>27</sup>A. De Wit, “Fingering of chemical fronts in porous media,” *Phys. Rev. Lett.* **87**, 054502 (2001).
- <sup>28</sup>A. De Wit, “Miscible density fingering of chemical fronts in porous media: Nonlinear simulations,” *Phys. Fluids* **16**, 163 (2004).
- <sup>29</sup>T. Bánsági, Jr., D. Horváth, Á. Tóth, J. Yang, S. Kalliadasis, and A. De Wit, “Density fingering of an exothermic autocatalytic reaction,” *Phys. Rev. E* **68**, 055301(R) (2003).
- <sup>30</sup>T. Bánsági, D. Horváth, and Á. Tóth, “Convective instability of an acidity front in Hele-Shaw cells,” *Phys. Rev. E* **68**, 026303 (2003).
- <sup>31</sup>S. Kalliadasis and G. M. Homsy, “Stability of free-surface thin-film flows over topography,” *J. Fluid Mech.* **448**, 387 (2001).
- <sup>32</sup>S. Kalliadasis, A. Kiyashko, and E. A. Demekhin, “Marangoni instability of a thin liquid film heated from below by a local heat source,” *J. Fluid Mech.* **475**, 377 (2003).
- <sup>33</sup>G. M. Homsy, “Viscous fingering in porous media,” *Annu. Rev. Fluid Mech.* **19**, 271 (1987).
- <sup>34</sup>J. Fernandez, P. Kurowski, P. Petitjeans, and E. Meiburg, “Density-driven unstable flows of miscible fluids in a Hele-Shaw cell,” *J. Fluid Mech.* **451**, 239 (2002).
- <sup>35</sup>M. C. Cross and P. C. Hohenberg, “Pattern formation outside of equilibrium,” *Rev. Mod. Phys.* **65**, 851 (1993).
- <sup>36</sup>G. Nicolis and I. Prigogine, *Self-Organization in Nonequilibrium Systems* (Wiley, New York, 1977).
- <sup>37</sup>*Chemical Waves and Patterns*, edited by R. Kapral and K. Showalter (Kluwer, Dordrecht, 1995).
- <sup>38</sup>A. De Wit, “Spatial patterns and spatiotemporal dynamics in chemical systems,” *Adv. Chem. Phys.* **109**, 435 (1999).
- <sup>39</sup>O. Manickam and G. M. Homsy, “Stability of miscible displacements in porous media with nonmonotonic viscosity profiles,” *Phys. Fluids A* **5**, 1356 (1993).
- <sup>40</sup>O. Manickam and G. M. Homsy, “Simulation of viscous fingering in miscible displacements with nonmonotonic viscosity profiles,” *Phys. Fluids* **6**, 95 (1994).
- <sup>41</sup>O. Manickam and G. M. Homsy, “Fingering instabilities in vertical miscible displacement flows in porous media,” *J. Fluid Mech.* **288**, 75 (1995).
- <sup>42</sup>C. T. Tan and G. M. Homsy, “Simulation of nonlinear viscous fingering in miscible displacement,” *Phys. Fluids* **31**, 1330 (1988).
- <sup>43</sup>Y. Ben, E. A. Demekhin, and H.-C. Chang, “A spectral theory for small-amplitude miscible fingering,” *Phys. Fluids* **14**, 999 (2002).
- <sup>44</sup>S. Fauve, “Pattern forming instabilities,” in *Hydrodynamics and Nonlinear Instabilities*, edited by C. Godrèche and P. Manneville (Cambridge University Press, Cambridge, 1998), p. 387.
- <sup>45</sup>P. Huerre and M. Rossi, “Hydrodynamic instabilities in open flows,” in *Hydrodynamics and Nonlinear Instabilities*, edited by C. Godrèche and P. Manneville (Cambridge University Press, Cambridge, 1998), p. 81.
- <sup>46</sup>J. Yang, Ph.D. thesis, University of Leeds, 2002.
- <sup>47</sup>R. A. Wooding, “Growth of fingers at an unstable diffusive interface in a porous medium or Hele-Shaw cell,” *J. Fluid Mech.* **39**, 477 (1969).
- <sup>48</sup>A. De Wit, P. De Kepper, K. Benyaich, G. Dewel, and P. Borckmans, “Hydrodynamical instability of spatially extended bistable chemical systems,” *Chem. Eng. Sci.* **58**, 4823 (2003).
- <sup>49</sup>F. Flouraboué and E. J. Hinch, “Kelvin–Helmholtz instability in a Hele-Shaw cell,” *Phys. Fluids* **14**, 922 (2002).
- <sup>50</sup>J. Martin, N. Rakotomalala, and D. Salin, “Gravitational instability of miscible fluids in a Hele-Shaw cell,” *Phys. Fluids* **14**, 902 (2002).
- <sup>51</sup>J. Martin, N. Rakotomalala, D. Salin, and M. Bockmann, “Buoyancy-driven instability of an autocatalytic reaction front in a Hele-Shaw cell,” *Phys. Rev. E* **65**, 051605 (2002).
- <sup>52</sup>R. Demuth and E. Meiburg, “Chemical fronts in Hele-Shaw cells: Linear stability analysis based on the three-dimensional Stokes equations,” *Phys. Fluids* **15**, 597 (2003).